The Importance of Electronic Dimensionality in Multi-Orbital Radical Conductors.

Aaron Mailman,[†, #,*] *Craig M. Robertson,*[⊥] *Stephen M. Winter,*[∀] *Paul A. Dube,*[^] *and Richard T. Oakley*[#,*]

Department of Chemistry, University of Jyväskylä, P.O. Box 35, Jyväskylä, Finland; Department of Chemistry, University of Waterloo, Waterloo, Ontario N2L 3G1, Canada; Department of Chemistry, University of Liverpool, Liverpool L69 7ZD, United Kingdom; Institut für Theoretische Physik, Goethe-Universität, Frankfurt am Main 60438, Germany; Brockhouse Institute for Materials Research, McMaster University, Hamilton, Ontario L8S 4M1, Canada.

Author email addresses: aaronmailman@gmail.com; oakley@uwaterloo.ca

Received Date:

Title Running Head: The Importance of Electronic Dimensionality in …

[†] University of Jyväskylä.
[#] University of Waterloo.
[⊥] University of Liverpool.
[∀] Goethe-Universität.
[^] McMaster University.

Abstract

The exceptional performance of oxobenzene-bridged bis-1,2,3-dithiazolyls **6** as single component neutral radical conductors arises from the presence of a low-lying π-LUMO, which reduces the potential barrier to charge transport and increases the kinetic stabilization energy of the metallic state. As part of ongoing efforts to modify the solid state structures and transport properties of these so-called multi-orbital materials we report the preparation and characterization of the acetoxy, methoxy and thiomethyl derivatives **6** (R = OAc, OMe, SMe). The crystal structures are based on ribbon-like arrays of radicals laced together by S···N′ and S···O′ secondary bonding interactions. The steric and electronic effects of the exocyclic ligands varies, affording 1D π-stacked radicals for R = OAc, 1D cofacial dimer π-stacks for R = SMe, and a pseudo 2D brick-wall arrangement for R = OMe. Variable temperature magnetic and conductivity measurements reveal strong antiferromagnetic interactions and Mott insulating behavior for the two radical-based structures (R = OAc, OMe), with lower room temperature conductivities ($\sigma_{RT} \sim 10^{-4}$ and $\sim 10^{-3}$ S cm^{-1} respectively) and higher thermal activation energies (E_{act} = 0.24 and 0.21 eV respectively) than found for the ideal 2D brick-wall structure of **6** (R = F), where $\sigma_{RT} \sim 10^{-2}$ S cm^{-1} and E_{act} = 0.10 eV. The performance of R = OMe, OAc relative to R = F is consistent with the results of DFT band electronic structure calculations, which indicate a lower kinetic stabilization energy of the putative metallic state arising from their reduced electronic dimensionality.

Introduction

Design strategies for conductive materials based on the use of neutral radicals as molecular building blocks can be traced back to the ideas of Haddon,[1] who applied Hubbard theory[2] to a model one-dimensional (1D) lattice composed of molecular radicals (Figure 1), each with one unpaired electron. Charge transport in such a system can be understood in terms of the competition between (i) the onsite Coulomb repulsion barrier U for charge transfer in the Mott insulating[3] state, which may be approximated in terms of the screened ionization energy (IP) and electron affinity (EA) of the radical, and (ii) the kinetic stabilization energy ΔE_k of the metallic state (Figure 1). The latter is a function of the hopping integral t_{ij} for charge migration between adjacent sites (i,j) and the related electronic bandwidth $W = 4|t_{ij}|$.[4] For a constant density of states,[5] the insulating and metallic states are degenerate when $U = W$. In organic solids, however, intermolecular interactions are notoriously weak, yielding small hopping integrals t_{ij} and narrow energy bands. Under these circumstances, when $W < U$, the unpaired electrons are trapped on the radicals, and a Mott insulating state prevails.

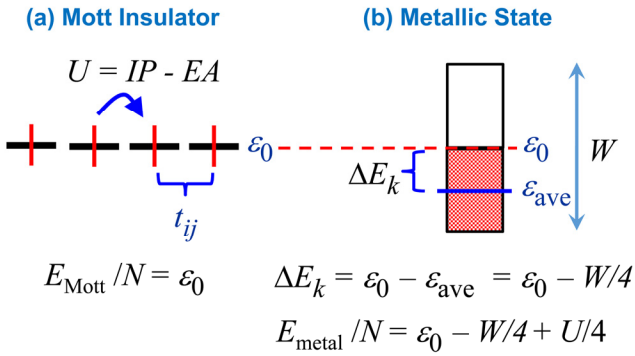

Figure 1. The single-orbital, single-electron Hubbard model applied to a 1D array of neutral radicals. (a) The Coulomb barrier U (= IP – EA), intersite hopping integral t_{ij} and orbital energy ε_0. (b) The kinetic stabilization energy ΔE_k of the metallic state expressed as the average energy ε_{ave} (= t_{ij} = W/4) of the band electrons relative to ε_0. Total energies per site of the insulating (E_{Mott}/N) and metallic (E_{metal}/N) states are degenerate when $W = U$.

Recognizing this energetic imbalance, Haddon proposed the use of the non-alternant hydrocarbon phenalenyl **1** (Chart 1) as a prototypal building block for a radical-based conductor (and superconductor),[1] reasoning that the Coulomb barrier U should be minimal since the unpaired electron occupies a purely non-bonding singly occupied molecular orbital (SOMO). In short, his approach was to accept the intrinsically low bandwidth W of organic (carbon-based) materials and to reduce the value of U to the point that $U < W$. Many variations on the phenalenyl framework have since been examined but, in the absence of steric blockage, dimerization through localized C-C σ-bonds or cofacial π-interactions is hard to avoid.[6,7,8] Moreover, estimates of U based on electrochemical data are relatively large. Its magnitude can be lowered by resonance effects, as in **2**,[9] in which spin density is partitioned between two phenalenyls, and even greater reductions are observed in spiro-conjugated internal salts such as **3**.[10,11] Some of these latter materials show impressively high, albeit activated conductivity, and resonating valence bond ground states have been proposed.[10c]

Chart 1

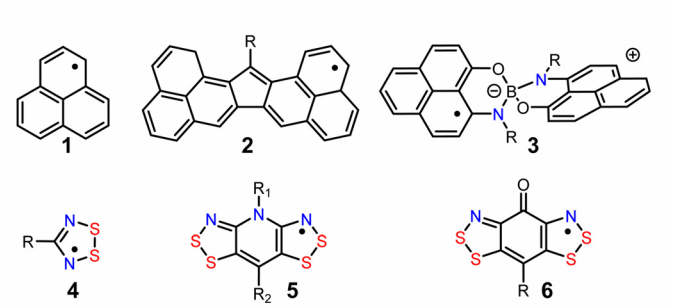

In contrast to work focused on purely carbon-based frameworks, our efforts towards the development of neutral radical conductors have been directed towards the use of heavy atom heterocycles, specifically those containing open shell thiazyl (SN) and selenazyl (SeN) units.[12,13] Just as in conductive radical-ion salts of donors such as tetrathiafulvalene,[14] where the presence of sulfur and/or its heavier congener selenium imparts both softness (a lower U) and increased orbital overlap (a larger t_{ij} and W), the introduction of heavy heteroatoms into molecular radicals can

improve their performance as conductors. However, many of the materials studied early on, notably those based on the dithiadiazolyl framework **4**, showed (in the absence of steric protection)[15] a strong tendency to associate in the solid state, resulting in insulating or weakly semiconducting behavior.[16] Metallic conductivity could be achieved by *p*-type doping,[17] but the challenge of improving charge transport *without* doping required greater spin delocalization to lower *U*. Synthetic efforts to this end eventually afforded *N*-alkylated pyridine-bridged bisdithiazolyls **5**,[18,19] in which not only was *U* markedly reduced but dimerization was also suppressed. While the conductivity of materials based on this resonance stabilized framework remained activated, with charge gaps Δ_C (= $U - W$) near 0.5 eV, replacement of sulfur by its heavier congener selenium[20] reduced Δ_C to the point that "bad metal" behavior ($E_{act} \sim 0$) could be achieved at pressures $P < 10$ GPa.[21] In addition, the selenium-based variants displayed strong isotropic and anisotropic magnetic exchange interactions,[22] affording magnetically ordered phases with high ordering temperatures and large coercive fields.[23,24]

As with phenalenyls, the charge transport in bisdithiazolyls **5** is well described in terms of the single-orbital Hubbard model shown in Figure 1; the magnitude of *U* and *W* depend only on the distribution of the radical SOMO, which dictates the values of *IP*, *EA* and intermolecular hopping integral t_{ij}. Replacement of the *N*-alkylpyridine bridge in **5** by an oxobenzene ring affords the seemingly similar framework **6**.[25] However, while the ground state electronic structures of bisdithiazolyls **5** and **6** are comparable, the values of *U* in **6** (estimated from electrochemical data)[25] are significantly smaller than those in **5**.[18,19a,b] The difference arises from the interaction of the low-lying π^*-acceptor orbital of the carbonyl group with the π-manifold of the radical,[26,27] which leads to a lowering of the LUMO of **6** relative to that of **5**. The presence of this low-lying virtual orbital in **6** (Figure 2) creates a multi-orbital effect[28] that opens up the electronic and magnetic

degrees of freedom available to the unpaired electron and destabilizes the Mott insulating state. In effect, the Coulomb barrier to charge transport is lowered from U to $U' = U - V + \Delta\varepsilon \pm K$, where $\Delta\varepsilon$ is the SOMO-LUMO gap, V represents the repulsion between electrons in different orbitals and K is the electron exchange term, the sign of which depends upon the spin state (triplet or open-shell singlet) afforded by electron transfer. Density functional theory (DFT) calculations on **6** (R = H) suggest a triplet ground state,[29a] with the corresponding value of U' being ~ 0.2 eV lower than U, in accord with electrochemical measurements. At the same time kinetic stabilization of the metallic state ΔE_k is increased as the Fermi level ε_F in the metallic state is lowered (from $\varepsilon_F = \varepsilon_0$) as electrons are redistributed between the SOMO and LUMO bands.[26a,29] The resulting shift in the chemical potential $\Delta\mu = \varepsilon_0 - \varepsilon_F$, combined with the dispersion term $\varepsilon_{dis} = \varepsilon_F - \varepsilon_{ave}$, affords $\Delta E_k = \varepsilon_{dis} + \Delta\mu$. The first term ε_{dis} is analogous to the dispersion stabilization in a single-orbital system ($W/4$ in Figure 1), but the chemical potential shift $\Delta\mu$ is a purely "multi-orbital" phenomenon.

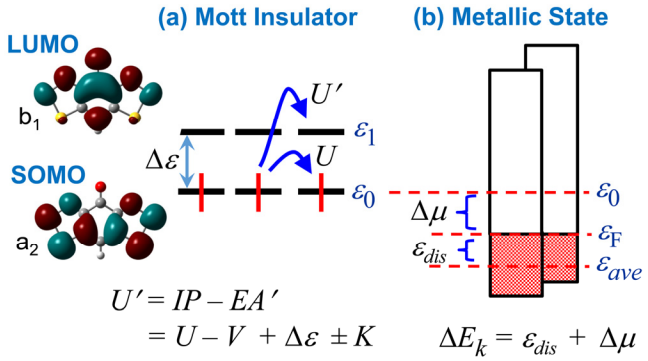

Figure 2. (a) Frontier orbitals and Coulomb barriers to intersite charge transfer U, U' along a 1D chain of multi-orbital oxobenzene-bridged bisdithiazolyl radicals **6** (R = H). U' is defined in terms of U (Figure 1), the SOMO-LUMO energy separation $\Delta\varepsilon$, electron repulsion V between electrons in different orbitals on the same site, and electron exchange K. (b) Schematic overlap of energy bands arising from combinations of the SOMO and LUMO, showing contributions to the kinetic stabilization ΔE_k of the metallic state afforded by (i) band dispersion $\varepsilon_{dis} = \varepsilon_F - \varepsilon_{ave}$, and (ii) electron redistribution $\Delta\mu = \varepsilon_0 - \varepsilon_F$ between the two bands.

In contrast to single-orbital radicals like **4**[30] and **5**[18], where U is largely independent of nature of the exocyclic ligand(s), as the SOMO is nodal at the sites of substitution, the exocyclic ligand R in multi-orbital radicals **6** plays an important electronic role since, while the SOMO remains nodal at the site of substitution, the LUMO is *not*. To a first approximation its orbital energy ε_1 is raised (or lowered) depending on the π-electron releasing (or accepting) power of the basal R-group. As a result the SOMO-LUMO separation $\Delta\varepsilon$ and hence the value of U' is not only small but *tunable*,[27] so that charge transport can be improved by substituent effects. Bad metal behavior has been induced in several radicals **6** (R = H, F, Ph, NO_2) at pressures ranging from 3-12 GPa.[25d,29]

From a solid state perspective the crystal structures of oxobenzene-bridged bisdithiazolyls are strongly influenced by intermolecular N/O$\cdots$ S′ secondary bonding interactions (SBIs)[31] (Figure 3a) that generate planar or near-planar ribbon-like arrays (Figure 3b) of radicals which can assemble in a variety of ways, to produce superimposed π-stacks, alternating ABABAB π-stacks, slipped π-stacks and brick-wall (R = F) architectures (Figure 3c-f). The dimensionality of the electronic structures arising from these packing motifs varies considerably, ranging from almost purely 1D (R = Ph, NO_2)[25a,27] to quasi-1D (R = Cl, H)[25c,e] and 2D (R = F).[25d] Of these, the 2D brick-wall pattern found for R = F provides the most effective kinetic stabilization of the metallic state; as such this material represents the "gold standard" for a neutral radical conductor. The small residual charge gap in this material (~0.1 eV) found at ambient pressure can be closed at 3 GPa, and further pressurization to 6 GPa affords a Fermi liquid state.[29b]

This latter finding, which represents the first observation of truly metallic behavior in a neutral radical conductor, has provided an incentive for continued exploration of multi-orbital radicals of this type, with the view of identifying specific structural motifs, notably the much sought-after[32] 2D brick-wall packing pattern. With this goal in mind we have prepared the acetoxy, methoxy and

thiomethyl derivatives **6** (R = OAc, OMe and SMe). As will be shown, these three radicals possess very different structures, ranging from 1D radical π-stacks for R = OAc to 1D dimer π-stacks for SMe and a *seemingly* 2D brick-wall architecture for R = OMe. Here we report details of these structures and the associated electronic and magnetic properties. The results are interpreted in the light of DFT band structure calculations, which provide insight into the electronic dimensionality of these materials.

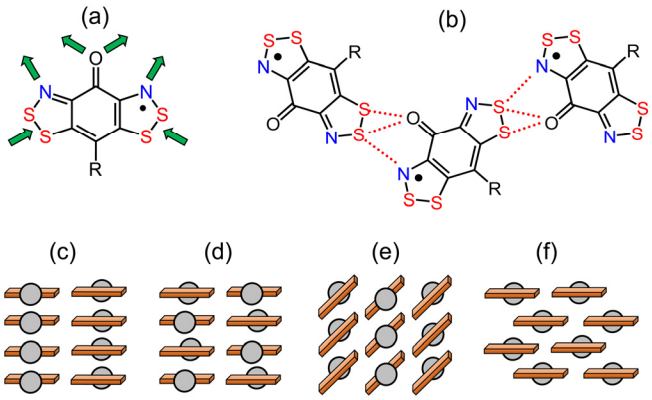

Figure 3. (a) Donor/acceptor sites in oxobenzene-bridged bisdithiazolyls **6**, and (b) resulting ribbon-like arrays of radicals linked by intermolecular N/O$\cdots$ S′ secondary bonding interactions. Packing of overlaid ribbons of **6** to afford (c) superimposed 1D π-stacks, (d) alternating ABABAB 1D π-stacks, (e) slipped quasi-1D π-stacks and (f) 2D brick-wall architectures.

Results and Discussion

Synthesis The starting point for the methoxy- and acetoxy-substituted radicals **6** (R = OMe, OAc) is the recently reported benzoquinone-bridged bisdithiazole zwitterion **7** (Scheme 1),[33] the framework of which is readily assembled by a double Herz condensation[34] of 2,6-diamino-1,4-dihydroxybenzene **8** (as its hydrochloride salt) with sulfur monochloride. The resulting salt [**7**][HCl] can be converted to the more soluble triflate salt by metathesis with trimethylsilyl triflate (TMSOTf). Subsequent deprotonation with Proton-Sponge yields neutral **7** which, upon

methylation with methyl triflate (MeOTf) affords the methoxy-substituted bisdithiazolylium salt [**6**][OTf] (R = OMe). Alternatively, acetylation of [**7**][HOTf] with acetic anhydride generates the acetoxy-substituted salt [**6**][OTf] (R = OAc). Finally, reduction of both the methoxy- and acetoxy-substituted salts [**6**][OTf] (R = OAc and OMe) with octamethylferrocene (OMFc) yields the respective radicals **6**. Thermal elimination of the methyl/acetyl group from **6** (R = OMe, OAc), to regenerate **7** can be achieved by heating either radical in the solid state in vacuo at 140 °C. Similar chemistry, leading to formation of a pyridone-bridged zwitterion, has been observed for the *N*-alkylpyridyl-bridged bisdithiazolyls **5** (R_1 = Me, R_2 = OMe).[35]

Scheme 1

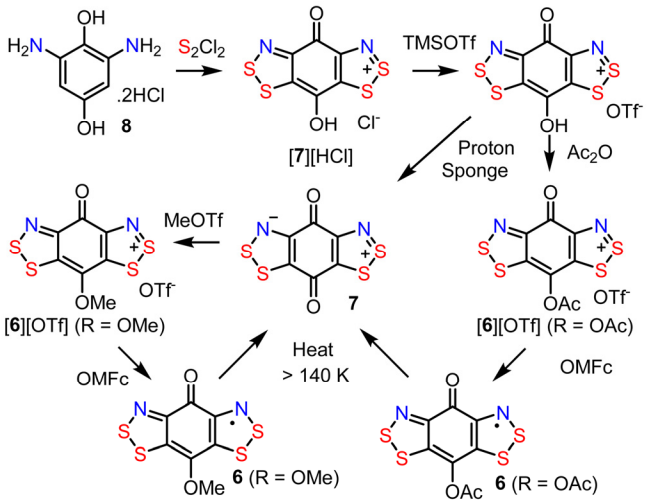

Synthesis of the thiomethyl-substituted radical **6** (R = SMe) follows a similar procedure (Scheme 2), involving double Herz condensation of 4-(methylthio)-2,6-diaminophenol bishydrochloride **9**, itself prepared by reduction of 4-(methylthio)-2,6-dinitrophenol, with sulfur monochloride. Metathesis of the resulting chloride salt [**6**][Cl] (R = SMe) with trimethylsilyl triflate affords the soluble triflate salt [**6**][OTf] (R = SMe), which can be reduced to the corresponding radical **6** (R = SMe) with octamethylferrocene (OMFc).

Scheme 2

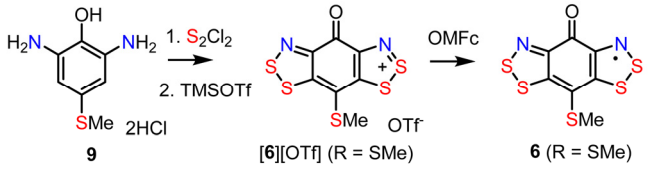

EPR Spectroscopy and Electrochemistry The three new radicals **6** (R = OAc, OMe and SMe) have been characterized in solution by X-band EPR spectroscopy (Figure 4). For R = OMe, OAc, strong, well-resolved spectra were obtained in degassed dichloromethane (DCM). In the case of R = SMe a DCM solution was EPR silent, a finding which may be related to the dimerization of this radical in the solid state (see below) and its subsequently low solubility. Pre-warming a sample of the dimer in toluene afforded a weak but broad signal. As in the case of the related radicals **6** (R = H, F, Cl, Ph, Me)[25] the spectra for R = OAc, OMe and SMe consist of a five-line pattern arising from hyperfine coupling to the two equivalent nitrogens [$I(^{14}N) = 1$], with a_N values typical of those found earlier.

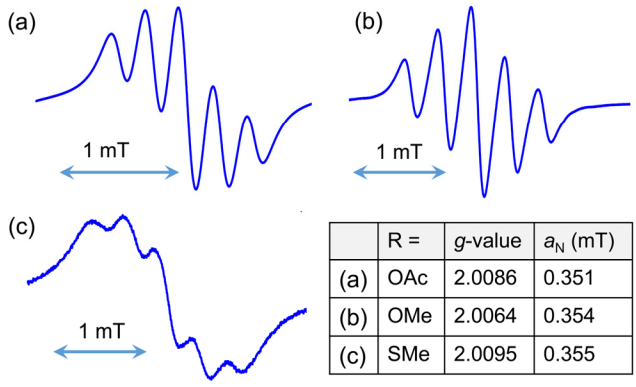

	R =	*g*-value	a_N (mT)
(a)	OAc	2.0086	0.351
(b)	OMe	2.0064	0.354
(c)	SMe	2.0095	0.355

Figure 4. X-band EPR spectra of radicals **6** with (a) R = OAc and (b) R = OMe in DCM and (c) R = SMe in toluene; spectral width = 3.0 mT.

The new radicals have also been examined using cyclic voltammetry (CV), to establish half-wave potentials for the (-1/0) and (0/+1) couples and the corresponding cell potential $E_{cell} = E_{½}(0/+1) –$

$E_{½}$(-1/0), which provides insight into the effective Coulomb barrier U'. A summary of potentials so obtained is provided in Table 1, along with corresponding data for related radicals **6** (R = Cl, F, H, NO_2) for comparison; relevant CV scans are illustrated in Figure S2. The (0/+1) wave is reversible in all cases, and the observed variation in $E_{½}$(0/+1) broadly speaking reflects the electron-withdrawing power of the ligand. With the exception of R = NO_2, SMe, the (-1/0) wave is irreversible, and for these non-ideal systems E_{cell} is estimated as the differences in the two cathodic peak potentials, that is, E_{pc}(0/+1) – E_{pc}(-1/0). As discussed earlier,[27,29b] the changes in E_{pc}(-1/0) and E_{cell} can be related the extent of π-interactions of the ligand R with the b_1 LUMO of the radical (Figure 2). Overall, the E_{cell} values for the R = OAc, OMe, SMe are all slightly smaller than that of R = F, suggesting that, to a first approximation, the values of U' should also be smaller.

Table 1. Electrochemical potentials[a] for selected radicals **6**.

R [b]	$E_{½}$(-1/0)	$E_{½}$(0/+1)	E_{cell} [d]
Cl	-0.481 [c]	0.194	0.64 [e]
F	-0.479 [c]	0.241	0.69 [e]
H	-0.525. [c]	0.072	0.56 [e]
NO_2	-0.218	0.227	0.45
OAc	-0.419 [c]	0.166	0.60 [e]
OMe	-0.571 [c]	0.131	0.67 [e]
SMe	-0.476	0.106	0.58

[a] In volts, measured on solutions of [**6**][OTf] in MeCN, referenced to SCE. [b] Data for R = Cl (ref 25c), F (ref 25d), H, (ref 25d), NO_2 (ref 27). [c] Reduction to the anion is irreversible; the cathodic peak potential E_{pc} is cited. [d] E_{cell} = $E_{½}$(0/+1) – $E_{½}$(-1/0). [e] E_{cell} estimated as E_{pc}(0/+1) – E_{pc}(-1/0).

Crystal Structures The crystal structures of the oxobenzene-bridged bisdithiazolyls **6** (R = OAc, OMe, SMe) have been determined by single crystal X-ray diffraction; crystal data are listed in Table S1. Selected intramolecular metrics, which are nominal for this class of compound, are provided in Table S2, and ORTEP drawings of the asymmetric units are shown in Figure 5.

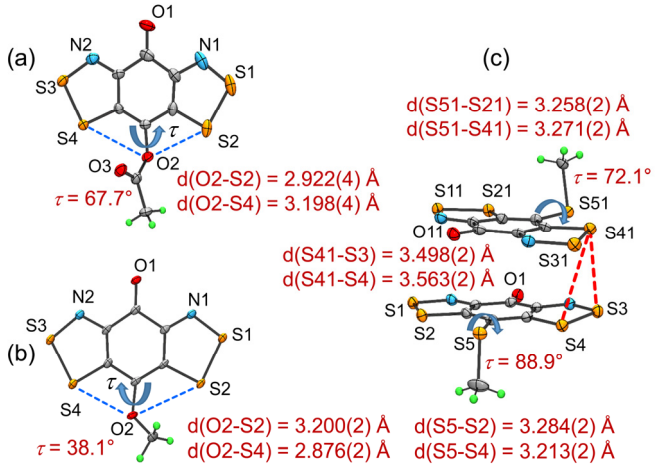

Figure 5. ORTEP drawings (50% probability ellipsoids at 100 K) of asymmetric units in **6** with (a) R = OAc, (b) R = OMe and (c) R = SMe. Torsion angles (τ), hypervalent ligand-to-ring contacts (blue) and interannular S···S distances for R = SMe (red) are highlighted.

At the molecular level, the three radicals differ only in the size and polarity of the basal ligand R. In all cases the ligand is rotated away from the plane of the radical. When R = OMe, the exocyclic C-O(CH_3) group generates a torsion angle $\tau = 38.1°$ with respect to the semiquinone ring, while for R = OAc $\tau = 67.7°$. This rotation gives rise to a slight inequality in the intramolecular O2···S2 and O2···S4 contacts, suggesting a slight hypervalent interaction on one side. In the R = SMe derivative there are two molecules in the asymmetric unit. These are aligned in a twisted trans-cofacial manner and mutually inclined so as to produce interannular S···S′ distances (Figure 5c) that are just inside the standard Van der Waals separation (3.6 Å) for two sulfur atoms.[36] The rotation of the two SMe groups is more extensive ($\tau = 72.1°$ and 89.9°) and there is little or no bias in the S5(1)···S2(1) and S5(1)···S4(1) contacts, indicating a negligible hypervalent effect.

We discuss the crystal structures of the three radicals starting with that of the acetoxy derivative **6** (R = OAc), which belongs to the orthorhombic space group $P2_12_12_1$; it is the simplest to describe and sets the stage for later comparisons. Views of the unit cell and packing are shown in Figure 6. The characteristic ribbon-like architecture is readily apparent, with neighboring radicals along the *y* direction laced together by short intermolecular O/N···S′ SBIs $d_{1,2}$. The bulky acetyl group plays two roles, serving partly as a structure maker, linking neighboring radical ribbons with intermolecular O···S′ SBIs (d_3 and d_4), but also as a buffer that separates radicals within the ribbons, so that the ribbons themselves are warped or ruffled away from planarity. A similar effect is observed in the structure of **6** (R = H),[25e] where intermolecular face-to-edge or "tilted-T" π-arene interactions[37] break up the otherwise planar arrays. In both cases, as a result of ruffling, lateral slippage of the ribbons is not possible, and the radicals are forced to adopt an isolated but uniformly spaced 1D AAAA slipped π-stack arrangement with interplanar spacing δ = 3.401Å.

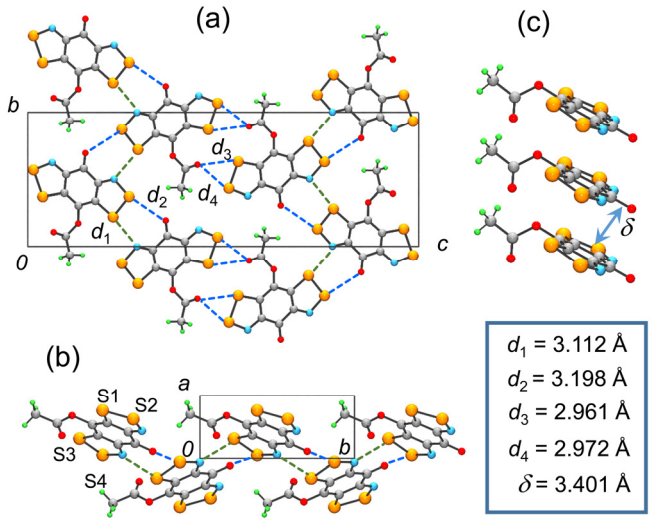

Figure 6. (a) Unit cell drawing of **6** (R = OAc), viewed parallel to the *a*-axis; lateral intermolecular S···O′ (blue) and S···N′ (green) SBIs $d_{1\text{-}4}$ are shown with dashed lines. (b) Ruffling of molecular ribbons in the *y* direction. (c) Tipped radical π-stacks, with interplanar separation δ.

Crystals of **6** (R = SMe) also belong to the orthorhombic space group $P2_12_12_1$ and, when viewed parallel to the *a*-axis, the unit cell (Figure 7) is reminiscent of that observed for the R = OAc derivative, with ribbons of radicals running along the *y* direction laced together by short intermolecular O/N···S′ contacts $d_{1\text{-}6}$. In this case, however, the SMe group does not serve as a structure maker, in that it does not generate close lateral intermolecular contacts. Instead its steric bulk leads not only to ruffling of the ribbons but also the formation of the weakly associated cofacial π-dimers shown in Figure 5 and a concomitant doubling of the *a* axis so as to afford an essentially 1D ABABAB slipped π-stack architecture.

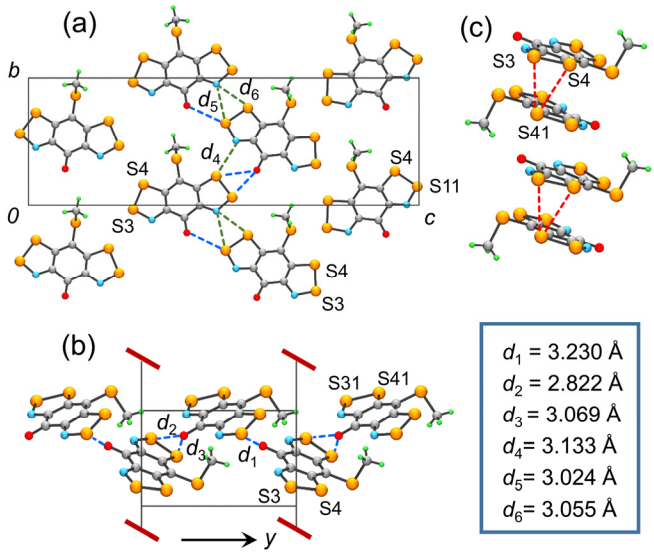

Figure 7. (a) Unit cell drawing of **6** (R = SMe), viewed parallel to the *a*-axis; lateral S···O′ (blue) and S···N′ (green) SBIs are shown with dashed lines. (b) Ruffling of molecular ribbons in the *y* direction. (c) Slipped π-stacks of dimers; S···S′ contacts (red) defined in Figure 5.

The crystal structure of **6** (R = OMe) belongs to the monoclinic space group $P2_1/c$ (Figure 8) and provides a marked contrast to those described above. While a ribbon-like arrangement of radicals linked by intermolecular O/N···S′ contacts $d_{1,2}$ is still observed, the relatively small size of the ligand combined with a small torsion angle τ is such that ruffling of the ribbons is not observed. Nonetheless the methoxy groups still play a steric role in partially separating neighboring ribbons, but the resulting close four-center S···S' contacts $d_{1,2}$ suggest a degree of lateral interactions along the y direction.

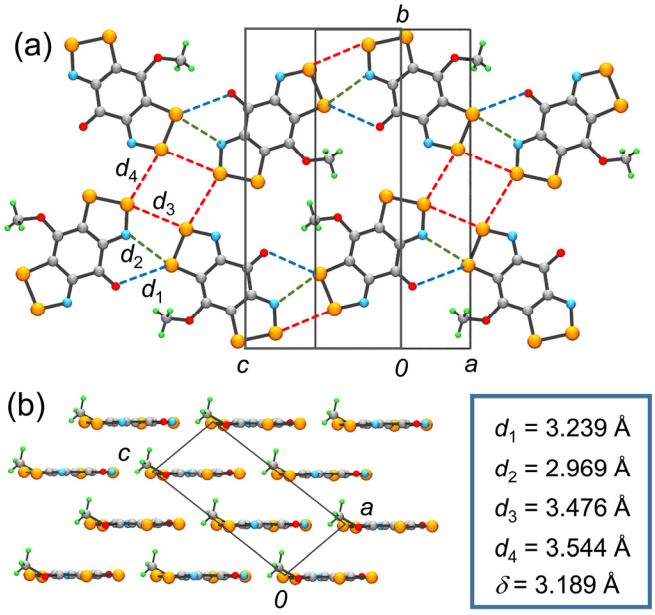

Figure 8. (a) Unit cell drawing of **6** (R = OMe), viewed perpendicular to the planes of the molecular ribbons; lateral S···O′ (blue), S···N′ (green) SBIs and S···S′ (red) contacts $d_{1\text{-}4}$ are shown with dashed lines; δ is the mean interplanar separation. (b) Slipped radical π-stacks running parallel to the a-axis.

The most striking feature of the structure of **6** (R = OMe) is the resemblance of the layering of the molecular ribbons to afford a brick-wall motif (Figure 3d) similar to that found for **6** (R = F).[25d] However, closer inspection reveals this similarity is only apparent. The high symmetry space group

*Cmc*2$_1$ found for R = F requires that each radical in the *xy* plane be surrounded by four equivalent neighbors, a *crystallographically* 2D arrangement associated with a single intermolecular contact 1 (Figure 9a). By contrast, in the lower symmetry structure found for R = OMe the four nearest neighbors fall into two pairs (Figure 9b), one involving sites related by translation (contact 1), the other sites related by *c*-glides (contact 2). Accordingly, the packing is more akin to that illustrated in Figure 3e, and the resulting electronic structure is perhaps better described as lying between a 1D and 2D system. That being said, the small interlayer spacing (δ = 3.189 Å) observed for R = OMe is close that found for R = F (δ = 3.151 Å),[25d] suggesting comparable interlayer hopping integrals associated with contact 1. However, a more meaningful comparison of the relative merits of the two packing arrangements requires analysis of their band electronic structures, to be described below.

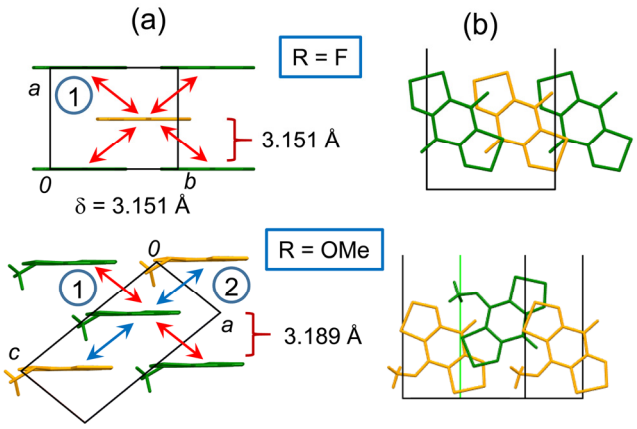

Figure 9. (a) Side and (b) top views of layering of ribbons in **6** with R = F and OMe, with alternate layers in green and yellow. For R = F, space group *Cmc*2$_1$, alternate layers are related by *C*-centering, and each radical has 4 equivalent neighbors (contact 1). For R = OMe, space group *P*2$_1$/*c*, neighboring layers are related by *c*-glides, with two distinct pairs of contacts (1 and 2).

Magnetic Susceptibility Measurements Previous work on the magnetic behavior of oxobenzene-bridged radicals **6** has revealed a remarkable tendency for strong ferromagnetic exchange interactions driven by Hund's rule coupling.[24,26] In many cases (R = F, H, Ph, Cl and I·EtCN)[25c,d,e,26b] these effects give rise bulk ordering as spin-canted antiferromagnets. However, DC magnetic susceptibility (χ) measurements on **6** (R = OAc, OMe) provide no indication of an FM response let alone magnetic ordering. Instead the results, illustrated in Figure 10a in the form of cooling curve plots of χT versus T over the range 2-300 K and measured using an external field of H = 1 kOe, reveal a strong, featureless antiferromagnetic (AFM) response, with the value of χT at 300 K lying well below that expected (0.375 emu K mol^{-1}) for a paramagnetic S = ½ system with a nominal value of $g \approx 2$. Perhaps not surprisingly, analogous behavior was observed for the structurally related radical **6** (R = Cl, as its MeCN solvate). In the case of **6** (R = SMe), AFM interactions are much stronger, with χT barely reaching 0.13 emu K mol^{-1} at 300 K. Moreover, on cooling to near 100 K, χT drops to a near-zero value, indicative of eventual complete association of the radicals into closed-shell singlet state.[19c]

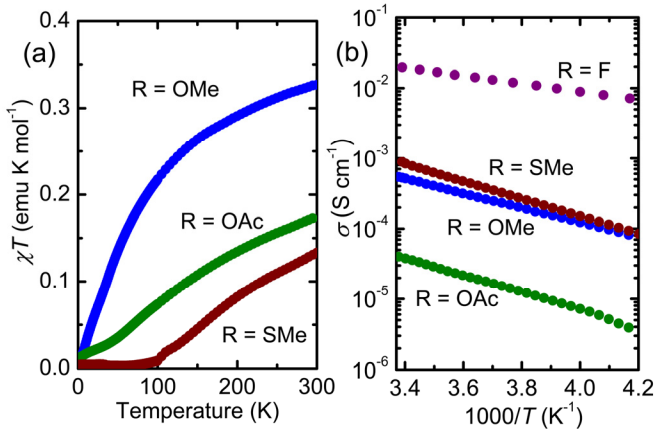

Figure 10. (a) Plots of χT (field cooled) versus T for **6** (R = OAc, OMe and SMe) at H = 1 kOe. (b) Plots of log σ versus 1000/T for **6** (R = OMe, OAc, SMe and F); data for R = F from ref 25d.

Conductivity Measurements Variable temperature conductivity measurements have been performed on **6** (R = OAc, OMe, SMe) using a four-probe technique on cold-pressed pellet samples. The results, presented in Figure 10b in the form of plots of log σ against $1/T$, along with corresponding data for R = F[25d] for purposes of comparison, indicate activated conductivity for all three materials. The values of the room temperature conductivity $\sigma_{RT} = 6 \times 10^{-5}$ S cm^{-1} (R = OAc), 6×10^{-4} S cm^{-1} (R = OMe) and 9×10^{-4} S cm^{-1} (R = SMe) are significantly lower than that found for R = F, where $\sigma_{RT} = 2 \times 10^{-2}$ S cm^{-1}. The corresponding Arrhenius activation energies E_{act} follow suit, with E_{act} decreasing along the series from 0.27 eV (R = SMe) to 0.24 eV (R = OAc), 0.21 eV (R = OMe) and 0.10 eV (R = F). In the case of R = SMe, where the magnetic data suggest a diamagnetic ground state, thermal activation may be related to the valence-to-conduction band gap E_g (= 2 E_{act}) of a conventional semiconductor. By contrast, the E_{act} values for R = OAc, OMe and F reflect the magnitude of the charge gap Δ_C between the Mott insulating and metallic states described above. The improvement in performance between R = OAc and OMe may thus be interpreted in terms of the increase in dimensionality noted in the crystallography, but the performance of the OMe derivative still falls well short of that displayed for R = F. This issue is discussed in detail in the following section.

Band Structure Calculations To explore and compare the solid state electronic structures of **6** (R= OMe, OAc, F) we have carried DFT band structure calculations using the Quantum Espresso package, with atomic coordinates taken from the crystal structures. The principal goal was to assess the relative electronic dimensionality of the three radicals, and to evaluate the kinetic stabilization energy E_k or effective bandwidth available to the putative metallic states for each system, and hence rationalize the $\sigma(1/T)$ profiles shown in Figure 10b. The band structures for all three radicals are presented in Figure 11 in the form of plots of crystal orbital (CO) dispersion

diagrams of the first Brillouin zone. The distribution of bands near the Fermi surface follows directly from frontier orbital pattern shown in Figure 2. Thus, in both R = OAc and R = OMe there are two prominent bands, each composed of four COs arising from mixtures of the a_2 SOMO and b_1 LUMO; the Fermi level resides in the lower band. Two heavily mixed bands are also observed in the R = F derivative, but because of *C*-centering there are only two COs per band.

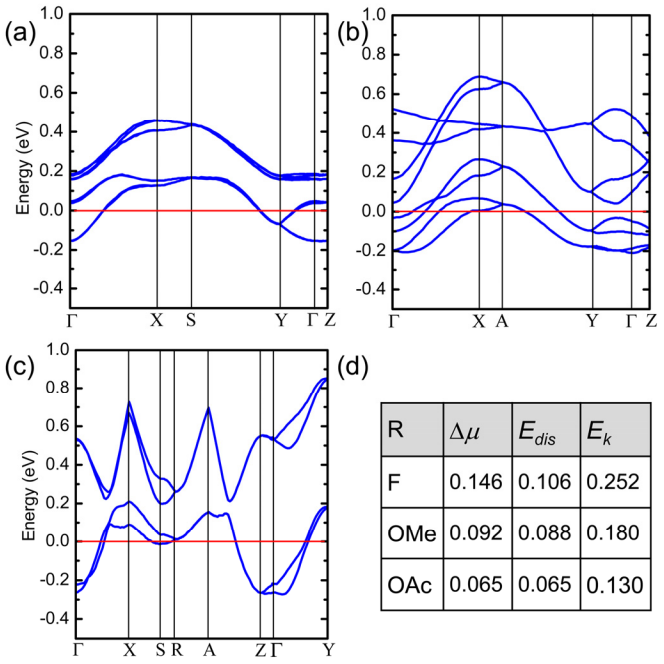

R	$\Delta\mu$	E_{dis}	E_k
F	0.146	0.106	0.252
OMe	0.092	0.088	0.180
OAc	0.065	0.065	0.130

Figure 11. Band dispersion diagrams for **6** with (a) R = OAc, (b) R = OMe and (c) R = F, assuming a metallic state, showing frontier crystal orbitals arising from mixtures of the SOMO and LUMO (Figure 2); the Fermi level (ε_F) is indicated with a red line. (d) Values of the multi-orbital redistribution term $\Delta\mu = \varepsilon_0 - \varepsilon_F$, the dispersion term $\varepsilon_{dis} = \varepsilon_F - \varepsilon_{ave}$ and the total kinetic stabilization energy $\Delta E_k = \varepsilon_{dis} + \Delta\mu$ (all in eV).

In accord with the above analysis of the crystal structure of the R = OAc derivative (space group $P2_12_12_1$), intermolecular interactions in this material are weak and highly 1D. Total CO dispersion in the lower band is greatest (near 0.34 eV) along the $\Gamma \rightarrow X$ vector, which corresponds precisely

to the π-stacking direction, weaker along $\Gamma \rightarrow Y$ (near 0.21 eV) and virtually negligible along from $\Gamma \rightarrow Z$. In the R = OMe derivative (space group $P2_1/c$) intermolecular interactions are stronger than for R = OAc. However, in spite of the appealing lamellar 2D-packing pattern its electronic structure remains largely 1D. Dispersion in the lower band along $\Gamma \rightarrow X$, which loosely speaking reflects the magnitude of hopping integrals along the slipped π-stacks (contact 1, Figure 9b), is significantly larger than along $\Gamma \rightarrow Y$, which derives from hopping between radicals related by *c*-glides (contact 2, Figure 9b). By contrast, in the R = F derivative (space group $Cmc2_1$) dispersion in both bands is strong along both $\Gamma \rightarrow X$ and $\Gamma \rightarrow Y$, in accord with the perfectly 2D brick-wall architecture illustrated in Figure 9a, whereby hopping integrals in the directions of the four nearest neighbor contacts (1) are all equal by symmetry.

As outlined in the introduction, we have previously demonstrated that the total kinetic stabilization energy of the putative metallic state of a multi-orbital radical ΔE_k can be expressed as the sum of two components (Figure 2), one ($\Delta\mu$) arising from a lowering of the Fermi level (ε_F) relative to the Mott state (ε_0) occasioned by electron redistribution between the SOMO and LUMO bands, the other stemming from the dispersion effects, that is, the delocalization of electrons within these bands (ε_{dis}), which lowers the average kinetic energy per electron (ε_{ave}) relative to ε_F.[26a,29] To illustrate the applicability of these concepts to the new radicals (R = OAc, OMe) we have carried out an analogous analysis of their band structures and the resulting density of states (Figure S2). Derived values of $\Delta\mu$, ε_{dis} and ΔE_k are presented in Figure 11d, along with those previously obtained for R = F. [26a,29] Overall, the results reveal the superiority of the 2D radical R = F, for which both the dispersive (ε_{dis}) and redistribution ($\Delta\mu$) terms are significantly greater than those found for R = OMe and, more particularly R = OAc. In fairness, it is noteworthy that ε_{dis} in R =

OMe and R = F are comparable, as a result of strong 1D interactions in the former, but with less SOMO-LUMO hybridization in R = OMe, $\Delta\mu$ falls well short of that found in R = F, so that the overall ΔE_k value is significantly lower. With even more weakly interacting 1D π-stacks and little SOMO-LUMO mixing, the R = OAc derivative falls short on both counts.

Summary and Conclusion

Within the language of the single-orbital, single-electron Hubbard model, high conductivity in organic radical-based materials is impeded by the energetic imbalance between the large potential energy cost (U) of site-to-site transfer of an unpaired electron and the limited kinetic stabilization energy (W) afforded by charge delocalization into a half-filled energy band. To break out of the Mott insulating state that this condition imposes, a variety of approaches have been pursued. The use of spin delocalization to lower U, as Haddon originally proposed,[1] and the incorporation of heavy heteroatoms (chemical pressure) to increase W, have both been extensively explored. Performance can also be improved by moving away from the classical one-orbital, one-electron model, as in mixed-valence spiroconjugated bis-phenalenyls[10,11] and chemically doped radical ion salts,[17] in which the effective Coulomb barrier is significantly reduced as additional channels for charge transport become available.

In oxobenzene-bridged bisdithiazolyl radicals **6** conductivity is enhanced by means of a multi-orbital effect, that is, the presence of a low-lying LUMO introduced by mixing of the radical π-manifold with the π-acceptor orbital of the exocyclic carbonyl group. The benefits are two-fold: (i) The Mott state is destabilized by lowering the Coulombic barrier U' to charge transport, and (ii) kinetic stabilization of the metallic state ΔE_k, that is, the effective bandwidth, is increased by mixing and hybridization of the SOMO and the LUMO, which lowers the Fermi level relative to

that of the Mott state. Together or separately, these two effects lead to a reduction in the charge gap Δ_C between the Mott insulating and metallic states. As such these purely organic materials provide an interesting comparison to open-shell (S = ½) Au(III) bis-dithiolate complexes,[38,39] where a multi-orbital effect emerges by virtue of a high-lying HOMO.

In terms of structure/property correlations, the crystal structures of **6** (R = OAc, OMe, SMe), like those of other oxobenzene-bridged radicals, are strongly influenced by intermolecular S···O′ and S···N′ SBIs which generate ribbon-like arrays of radicals. However, the steric and electronic demands of the ligands also play an important role. When R = OAc, the acetyl group causes severe ruffling of the ribbons, but also maintains regularity of the spacing between the layers by means of SBI effects, so as to produce a highly 1D AAAA π-stacked architecture. By contrast, when R = SMe, there are no SBI effects, but the steric demands of the ligand leads to the formation of ABABAB dimer π-stacks. Finally, in the R = OMe derivative, steric and SBI effects involving the ligand are both minimal, and ribbon ruffling is not observed. Instead, slippage and layering of the ribbons results in a lamellar packing motif which provides an appealing but strong but illusory resemblance to the perfectly 2D brick-wall architecture found for the R = F material. DFT band structure calculations indicate that its electronic structure is better described as being more nearly 1D. The extent of SOMO-LUMO mixing is decreased, and the resulting contributions ε_{dis} and $\Delta\mu$ to the overall kinetic stabilization energy ΔE_k for R = OMe are significantly smaller than for R = F, leading to a larger charge gap Δ_C, notwithstanding the smaller U' suggested by the E_{cell} measurements. By virtue of the high kinetic stabilization energy of its metallic state, the R = F radical remains the "gold standard" as a neutral radical conductor.[29b] Investigations of the transport properties of this latter material are ongoing.

Experimental Section

General Methods and Procedures. The reagents sulfur monochloride, octamethylferrocene (OMFc), trimethylsilyl triflate (TMSOTf), methyl triflate (MeOTf) and Proton-Sponge were obtained commercially. OMFc was sublimed in vacuo and recrystallized from acetonitrile before use. The hydrochloride salt [**7**][HCl] was prepared by the condensation of 1,4-dihydroxy-2,6-diaminobenzene **8** (as bishydrochloride salt) with sulfur monochloride;[33] the corresponding triflate salt was obtained by metathesis with TMSOTf. 4-(Methylthio)-2,6-dinitrophenol **9** was prepared according a modification of a literature procedure.[40] The solvents acetonitrile (MeCN), dichloroethane (DCE), dichloromethane (DCM) were of at least reagent grade; MeCN was dried by distillation from P_2O_5 and CaH_2, DCE and DCM by distillation from P_2O_5. All reactions were performed under an atmosphere of dry nitrogen. Melting points are uncorrected. Infrared spectra (Nujol mulls, KBr optics) were recorded on a Nicolet Avatar FTIR spectrometer at 2 cm^{-1} resolution, and ^1H NMR spectra were run on a Bruker Avance 300 MHz NMR spectrometer and low resolution Electro-Spray Ionization (ESI) mass spectra were recorded on a Micromass Q-TOF Ultima Global LC/MS/MS system. Elemental analyses were performed by MHW Laboratories, Phoenix, AZ 85018 or carried out in-house on an Elementar Vario EL III elemental analyzer.

Preparation of [6][OTf] (R = OAc). A slurry of [**7**][HOTf] (0.405 g, 0.987 mmol) in 25 mL of acetic anhydride was heated at gentle reflux for 1.5 h. The mixture was then hot filtered and cooled to -20 °C to afford copper flakes of [**6**][OTf] (R = OAc) which were collected by filtration, washed with 2 × 20 mL of DCM and dried in vacuo. Yield 0.416 g (0.919 mmol, 93 %); mp > 250 ºC. Anal. Calcd for $C_9H_3F_3N_2O_6S_5$: C, 23.89; H, 0.67; N, 6.19. Found: C, 23.66; H, 1.00; N, 5.96. IR (Nujol mull, KBr, cm^{-1}): 3353 (vw), 1770 (vs), 1683 (vs), 1269 (s), 1240 (s), 1220 (s), 1160 (vs),

1108 (s), 1026 (s), 878 (m), 858 (m), 845 (m), 780 (s), 754 (s), 637 (s), 604 (m), 588 (w), 572 (m), 518 (m), 506 (m), 488 (m), 479 (m), 464 (w), 410 (w).

Preparation of 6 (R = OAc). A degassed solution of [**7**][OTf] (R = OAc) (0.395 g, 0.873 mmol) in MeCN (three freeze-pump-thaw cycles) was tipped onto solid OMFc (0.312 g, 1.046 mmol) and the mixture stirred at room temperature for 1 h. The resulting black needles of [**7**] (R = OAc), which were suitable for single crystal X-ray diffraction and transport property measurements, were collected by filtration, washed with 3 × 7 mL MeCN and dried in vacuo; yield 0.226 g (0.745 mmol, 85%). Anal. Calcd for $C_9H_3N_2O_3S_4$: C, 31.67; H, 1.00; N, 9.23. Found: C, 31.42; H, 1.12; N, 9.10. IR (Nujol mull, KBr, cm^{-1}): 1742 (vs), 1643 (vs), 1203 (vs), 1123 (m), 1097 (m), 1035 (s, br), 876 (m), 839 (w), 819 (vw), 772 (vw), 753 (m), 734 (s), 668 (vw), 621 (w), 599 (w), 518 (m), 471 (w), 460 (m).

Preparation of [6][OTf] (R = OMe). To a solution of Proton-Sponge (0.218 g, 1.017 mmol) in 30 mL of DCE was added an excess of MeOTf (0.580 g, 3.534 mmol) and the mixture stirred at room temperature for 15 min. Finely powdered zwitterion **7** (0.252 g, 0.968 mmol) was added and the resulting slurry stirred and heated to a gentle reflux under argon for 68 h. The purple-brown microcrystalline solid of crude [**6**][OTf] (R = OMe) was filtered off, washed with DCM and dried in vacuo. This crude solid was stirred in 30 mL of MeCN and an excess of 3-cyanopyridine (0.318 g, 3.050 mmol) added and the mixture stirred at room temperature for 1 h, filtered to remove the insoluble **7** and the volatiles flash distilled. The solid was triturated with a 3:1 (v/v) mixture of DCM and MeCN, filtered, washed with 5 × 15 mL of DCM and collected by filtration and air dried to afford 0.289 g of crude [**6**][OTf] (R = OMe). Repeated recrystallization from a small volume of EtCN afforded bronze needles. Yield 0.105 g (0.247 mmol, 26 %); mp > 250 °C. Anal. Calcd for $C_8H_3F_3N_2O_5S_5$: C, 22.64; H, 0.71; N, 6.60. Found: C, 23.00; H, 0.89; N, 6.72. IR (Nujol mull, cm^{-}

^{1}): 1684 (s), 1432 (vs), 1407 (s), 1319 (w), 1288 (m), 1261 (m), 1237 (vs), 1167 (s), 1127 (w), 1103 (m), 1023 (s), 997 (w), 929 (m), 854 (m), 780 (s), 742 (m), 635 (s), 574 (m), 517 (m), 476 (m). ^{1}H NMR (300 MHz, CD_3CN): 4.06 (s, 3H).

Preparation of 6 (R = OMe). Method A. *Crystal growth by slow diffusion.* [**6**][OTf] (R = OMe) (47 mg, 0.111 mmol) in 7 mL of degassed MeCN (four freeze-pump-thaw cycles) was allowed to diffuse slowly into a similarly degassed solution of OMFc (51 mg, 0.171 mmol) in 7 mL of MeCN over 16 h, to afford **6** (R = OMe) as small black needles. **Method B.** *Bulk reduction for conductivity and magnetic susceptibility.* Neat MeCN (15 mL) was degassed by four freeze-pump-thaw cycles and tipped onto solid [**6**][OTf] (R = OMe) (214 mg, 0.504 mmol) and OMFc (189 mg, 0.634 mmol) and the mixture stirred at 0-5 °C for 2 h. The microcrystalline purple solid was collected by filtration, washed with 5 × 10 mL MeCN and dried in vacuo to afford **7** (R = OMe) in 81 % yield (112 mg, 0.407 mmol). Anal. Calcd for $C_7H_3N_2O_2S_4$: C, 30.53; H, 1.10; N, 10.17. Found: C, 30.43; H, 1.29; N, 9.84. IR (Nujol mull, cm^{-1}): 1639 (vs), 1526 (w), 1404 (m), 1337 (m), 1263 (m), 1191 (m), 1114 (vs, br), 1057 (s, br), 980 (w), 916 (w), 830 (w), 801 (w), 753 (m), 711 (s), 627 (m), 531 (m), 490 (w), 469 (m), 434 (w).

Preparation of 4-(Methylthio)-2,6-diaminophenol Bishydrochloride, 9. Tin powder (13.11 g, 110.4 mmol) was added in small portions over 1 h to a mixture of **4** (10.01 g, 43.47 mmol) and $SnCl_2(H_2O)_2$ (19.78 g, 87.68 mmol) in 250 mL conc. HCl at 20 °C. The mixture was stirred for an additional 2 h at 20 °C, then filtered through a glass Buchner funnel and the filtrate concentrated under reduced pressure to a thick yellow-white paste. This paste was triturated with 50 mL conc. HCl and the resulting white solid collected by filtration and air dried. Repeated recrystallization from 1:2 (v/v) H_2O/HCl gave cream colored needles of **9**; yield 4.76 g (19.6 mmol, 45 %); dec > 200 °C. Anal. Calcd for $C_7H_{12}Cl_2N_2OS$: C, 34.58; H, 4.97; N, 11.52. Found C, 34.14; H, 5.05; N,

11.37. IR (Nujol mull, cm^{-1}): 3424 (br, s), 3253 (s), 2199 (w), 2076 (w), 1950 (br, vs), 1738 (w), 1640 (w), 1564 (s), 1490 (s), 1301 (m), 1275 (m), 1235 (s), 1129 (m), 1101 (m), 1045 (w), 994 (w), 964 (m), 901 (w), 883 (w), 862 (m), 759 (m), 709 (m), 636 (s), 595 (m), 578 (w), 540 (w), 516 (w).

Preparation of [6][Cl] (R = SMe). Neat sulfur monochloride (6.45 g, 30.6 mmol) was added dropwise to a suspension of **9** (1.84 g, 7.85 mmol) in 50 mL anhydrous MeCN and the mixture gently refluxed for 16 h under an atmosphere of N_2. The black solid was filtered off, washed with MeCN, hot DCE, then DCM and finally dried *in vacuo*. Yield 2.34 g (7.16 mmol, 91%); mp > 250 ^{o}C. IR (Nujol mull, cm^{-1}): 1664 (vs), 1406 (s), 1313 (w), 1292 (w), 1270 (vs), 1099 (s), 1063 (w), 1023 (m), 969 (m), 908 (w), 847 (w), 824 (m), 761 (s), 637 (w), 607 (m), 484 (s).

Preparation of [6][OTf] (R = SMe). TMSOTf (1.94 g, 8.73 mmol) was added to a slurry of crude [**6**][Cl] (R = SMe) (2.34 g, 7.31 mmol) in 50 mL of MeCN, to afford a deep purple solution that was stirred at room temperature for 1 h. The purple-black solid was filtered off, washed with 2 × 15 mL MeCN and dried *in vacuo* to give crude [**6**][OTf] (R = SMe) (1.51 g). The solvent was flash distilled from the filtrate to give an additional 1.39 g of crude product; overall yield 2.90 g (6.59 mmol, 92%). Repeated recrystallization from MeCN afforded lustrous copper needles of [**6**][OTf] (R = SMe), dec > 220 $^{\circ}$C. Anal. Calcd for $C_8H_3F_3N_2O_4S_6$: C, 21.81; H, 0.69; N, 6.36. Found: C, 22.00, H, 0.57; N, 6.53. IR (Nujol mull, cm^{-1}): 1693 (sh, m), 1683 (s), 1402 (m), 1294 (m), 1271 (s), 1247 (s), 1234 (s), 1219 (m), 1152 (vs), 1092 (m), 1023 (s), 966 (m), 854 (w), 833 (vw), 823 (w), 781 (m), 771 (m), 634 (s), 608 (w), 573 (m), 516 (m), 501 (m), 486 (m).

Preparation of [6][R = SMe]. *Bulk reduction for conductivity and magnetic susceptibility*. A solution of [**6**][OTf] (R = SMe) (0.270 g, 0.613 mmol) in 30 mL of MeCN was degassed by four freeze-pump-thaw cycles and was tipped into a similarly degassed solution of OMFc (0.270 g,

0.906 mmol) in 30 mL of MeCN. The mixture was stirred at room temperature for 1 h and the microcrystalline purple solid was collected by filtration, washed with 4 × 15 mL MeCN and dried in vacuo to afford **6** (R = SMe); yield 129 mg (0.443 mmol, 72%). Anal. Calcd for $C_7H_3N_2O_2S_5$: C, 28.85; H, 1.04; N, 9.61. Found: C, 28.51; H, 1.26; N, 9.75. IR (Nujol mull, cm^{-1}): 3068 br, s, 1595 vs, 1526 s, 1306 s, 1271 m, 1225 m, 1169 w, 1102 vs, 1016 w, 967 m, 895 w, 850 w, 827 m, 761 w, 636 w, 536 w, 494 m, 489 w, 460 m.

Cyclic Voltammetry. Cyclic voltammetry was performed using a Gamry Reference 600 Potentiostat/Galvanostat/ZRA with two consecutive scans of 100 - 200 mV s^{-1} (maximum current 50 μA) on solutions of [**6**][OTf] (R = OAc, OMe, SMe) in MeCN (dried by successive fractional distillation from P_2O_5 and CaH_2 under argon atmosphere) containing 0.1 M tetra-*n*-butylammonium hexafluorophosphate (*n*-Bu_4NPF_6) as supporting electrolyte under an argon atmosphere. Potentials (Table 1 and Figure S2) were scanned with respect to quasi-reference electrode in a single compartment cell fitted with Pt electrodes and referenced to the Fc/Fc^+ couple of ferrocene at 0.38 V *vs* SCE.[41] The E_{pa}-E_{pc} separation of the reversible couples were within 10% of that of the Fc/Fc^+ couple.

EPR Spectroscopy. X-Band EPR spectra of **6** (R = OAc, OMe, SMe) were recorded at ambient temperature on a Bruker EMX-200 spectrometer using samples dissolved in degassed DCM (R = OAc, OMe) or toluene (R = SMe). Hyperfine coupling constants were obtained by spectral simulation using Simfonia[42] and WinSim.

Crystallography. Crystals of **6** (R = OAc, OMe, SMe) were mounted on a MiTeGen MicroMount using Fomblin oil. Diffraction data were measured at 100 K on beamline I19 at the Diamond Light Source (λ = 0.6889 Å), collected using Rigaku CrystalClear[43] software and

processed with APEX2 software[44] and SADABS.[45] Structural solution and least square refinements were conducted using the OLEX2[46] interface to the SHELX suite.

Magnetic Susceptibility Measurements. DC magnetic susceptibility (χ) measurements on **6** (R = OAc, OMe, SMe) were performed over the temperature range 2-300 K on a Quantum Design MPMS SQUID magnetometer. Diamagnetic corrections were made using Pascal's constants.[47]

Conductivity Measurements. Four-probe temperature dependent conductivity measurements on cold-pressed pellet (1 × 1 × 5 mm) samples of **6** (R = OAc, OMe, SMe) were performed over the range T = 200-300 K using home-built equipment. Silver paint (Leitsilber 200) was used to apply the electrical contacts. For convenience, the term σ_{RT} refers to the conductivity at T = 295 K.

Electronic Structure Calculations. DFT band structure calculations on **6** (R = OMe, OAc, F) were based on atomic coordinates taken from crystallographic data, and used the Quantum Espresso package[48] with ultrasoft PBE pseudopotentials[49] and a plane-wave cutoff of 25 Ry and a 250 Ry integration mesh. The SCF calculations employed a 4 × 4 × 4 Monkhorst−Pack k-point mesh, and were performed assuming a nonmagnetic (metallic) state. The band dispersion diagrams in Figure 11 are based on k-point grids available on the Bilbao Crystallographic Server.[50] The results for R = OAc, OMe were further analyzed using the WANNIER90 code[51] to generate a tight-binding model including the SOMO energy ε_0, which was obtained after rotation of the resulting Hamiltonian into diagonal form at each site. The resulting density of states are shown in Figure S2, along with values of ε_0, ε_F and ε_{ave}, as well as $\Delta\mu$, ε_{dis} and ΔE_k derived as described previously.[26a,29b]

Supporting Information. The Supporting Information is available free of charge on the ACS Publications website at DOI: 10.1021/xxx.xxxxx.

Details of X-ray data collection, CCDC codes, CV scans and density of states calculations (PDF).

CCDC 1902028-1902030 contain the supplementary crystallographic data for this paper. These data can be obtained free of charge via www.ccdc.cam.ac.uk/data_request/cif, or by emailing data_request@ccdc.cam.ac.uk, or by contacting The Cambridge Crystallographic Data Centre, 12 Union Road, Cambridge CB2 1EZ, UK; fax: +44 1223 336033.

Corresponding Authors

aaronmailman@gmail.com; oakley@uwaterloo.ca

ORCID

Aaron Mailman: 0000-0003-2067-8479

Craig M. Robertson: 0000-0002-4789-7607

Richard T. Oakley: 0000-0002-7185-2580

Notes. The authors declare no competing financial interest.

Acknowledgement. This work was supported by the Natural Sciences and Engineering Research Council of Canada (NSERCC), the University of Jyväskylä, the Academy of Finland (projects 253907 and 289172) and the European Union's H2020 research and innovations programme (under the Marie Skłodowska-Curie Grant Agreement 659123). A.M. is grateful for the interest and support of Prof. Heikki M. Tuononen during this research. We also thank the Diamond Light Source for access to beamline I19.

References

[1] (a) Haddon, R. C. *Nature* **1975**, *256*, 394. (b) Haddon, R. C. *Aust. J. Chem*. **1975**, *28*, 2333. (c) Haddon, R. C. *Aust. J. Chem*. **1975**, *28*, 2343. (d) Haddon, R. C. *ChemPhysChem* **2012**, *13*, 3581.

[2] Hubbard, J. *Proc. R. Soc. London, Ser. A* **1963**, *276*, 238.

[3] (a) Mott, N. F. *Proc. Phys. Soc., London, Sect. A* **1949**, *62*, 416. (b) Mott, N. F. Metal-Insulator Transitions; Taylor and Francis: London, 1990.

[4] In higher dimensional systems, the relationship $W = 4zt$, where $z = 1$, 2 or 3, applies. See Kaxiras, E. *Atomic and Electronic Structure of Solids*; Cambridge University Press: 2003.

[5] A more rigorous treatment of a half-filled 1D band which does not assume a uniform distribution of energy levels affords $\varepsilon_{ave} = (4/\pi)t_{ij}$. See Whangbo, M. H. Mott-Hubbard condition for electron localization in the Hartree-Fock band theory. *J. Chem. Phys*. **1979**, *70*, 4763.

[6] (a) Morita, Y.; Suzuki, S.; Sato, K.; Takui, T. Synthetic organic spin chemistry for structurally well-defined open-shell graphene fragments. *Nat. Chem*. **2011**, *3*, 197. (b) Kubo, T. Phenalenyl-based open-shell polycyclic aromatic hydrocarbons. *Chem. Rec.* **2015**, *15*, 218.

[7] (a) Goto, K.; Kubo, T.; Yamamoto, K.; Nakasuji, K.; Sato, K.; Shiomi, D.; Takui, T.; Kubota, M.; Kobayashi, T.; Yakusi, K.; Ouyang, J. A Stable Neutral Hydrocarbon Radical: Synthesis, Crystal Structure, and Physical Properties of 2,5,8-Tri-*tert*-butyl-phenalenyl. *J. Am. Chem. Soc*. **1999**, *121*, 1619. (b) Koutentis, P. A.; Chen, Y.; Cao, Y.; Best, T. P.; Itkis, M. E.; Beer, L.; Oakley, R. T.; Brock, C. P.; Haddon, R. C. Perchlorophenalenyl Radical. *J. Am. Chem. Soc*. **2001**, *123*, 3864. (c) Beer, L.; Mandal, S. K.; Reed, R. W.; Oakley R. T.; Tham, F. S.; Donnadieu, B.; Haddon, R. C. The First Electronically Stabilized Phenalenyl Radical: Effect of Substituents on Solution Chemistry and Solid-State Structure. *Cryst. Growth Des.* **2007**, *7*, 802. (d) Mou, Z.; Uchida, K.; Kubo, T.; Kertesz, M. Evidence of σ- and π-Dimerization in a Series of Phenalenyls. *J. Am. Chem. Soc.* **2014**, *136*, 18009. (e) Kertesz, M. Pancake Bonding: An Unusual Pi-Stacking Interaction. *Chem.-Eur. J.* **2019**, *25*, 400.

[8] (a) Uchida, K.; Mou, Z.; Kertesz, M.; Kubo, T. Fluxional σ-Bonds of the 2,5,8-Trimethylphenalenyl Dimer: Direct Observation of the Sixfold σ-Bond Shift via a π-Dimer. *J. Am. Chem. Soc*. **2016**, *138*, 4665. (c) Nishida, S.; Kawai, J.; Moriguchi, M.; Ohba,T.; Haneda, N.; Fukui, K.; Fuyuhiro, A.; Shiomi, D.; Sato, K.; Takui, T.; Nakasuji, K.; Morita, Y. Control of Exchange Interactions in π-Dimers of 6-Oxophenalenoxyl Neutral π-Radicals: Spin-Density Distributions and Multicentered Two-Electron Bonding Governed by Topological Symmetry and Substitution at the 8-Position. *Chem.-Eur. J.* **2013**, *19*, 11904. (d) Cui, Z. H.; Gupta, A.; Lischka, H.; Kertesz, M. *Phys. Chem. Chem. Phys.* **2015**, *17*, 23963. (e) Kolb, B.; Kertesz, M.; Thonhauser, T. Concave or convex π-dimers: the role of the pancake bond in substituted phenalenyl radical

dimers. *J. Phys. Chem. A* **2013**, *117*, 3642. (f) Small, D.; Zaitsev, V.; Jung, Y.; Rosokha, S. V.; Head-Gordon, M.; Kochi, J. K. Intermolecular π-to-π Bonding between Stacked Aromatic Dyads. Experimental and Theoretical Binding Energies and Near-IR Optical Transitions for Phenalenyl Radical/Radical versus Radical/Cation Dimerizations. *J. Am. Chem. Soc*. **2004**, *126*, 13850. (g) Beer, L.; Reed, R. W.; Robertson, C. M.; Oakley, R. T.; Tham, F. S.; Haddon, R. C. Tetrathiophenalenyl Radical and its Disulfide-Bridged Dimer. *Org. Lett*. **2008**, *10*, 3121.

[9] (a) Kubo, T.; Katada, Y.; Shimizu, A.; Hirao, Y.; Sato, K.; Takui, T.; Uruichi, M.; Yakushi, K.; Haddon, R. C. Synthesis, Crystal Structure, and Physical Properties of Sterically Unprotected Hydrocarbon Radicals. *J. Am. Chem. Soc.* **2011***, 133*, 14240. (b) Wehrmann, C. M.; Charlton, R. T.; Chen, M. S. A Concise Synthetic Strategy for Accessing Ambient Stable Bisphenalenyls toward Achieving Electroactive Open-Shell π-Conjugated Materials. *J. Am. Chem. Soc*. **2019**, *141*, 3240.

[10] (a) Chi, X.; Itkis, M. E.; Patrick, B. O.; Barclay, T. M.; Reed, R. W.; Oakley, R. T.; Cordes, A. W.; Haddon, R. C. The First Phenalenyl-Based Neutral Radical Molecular Conductor. *J. Am. Chem. Soc*. **1999**, *121*, 10395. (b) Huang, J.; Kertesz, M. Spin Crossover of Spiro-Biphenalenyl Neutral Radical Molecular Conductors. *J. Am. Chem. Soc*. **2003**, *125*, 13334. (c) Mandal, S. K.; Samanta, S.; Itkis, M. E.; Jensen, D. W.; Reed, R. W.; Oakley, R. T.; Tham, F. S.; Donnadieu, B.; Haddon, R. C. Resonating Valence Bond Ground State in Oxygen-Functionalized Phenalenyl-Based Neutral Radical Molecular Conductors. *J. Am. Chem. Soc*. **2006**, *128*, 1982. (d) Mandal, S. K.; Itkis, M. E..; Chi, X.; Samanta, S.; Lidsky, D.; Reed, R. W.; Oakley, R. T.; Tham, F. S.; Haddon, R. C. New family of aminophenalenyl-based neutral radical molecular conductors: Synthesis, structure, and solid state properties. *J. Am. Chem. Soc.* **2005**, *127*, 8185. (e) Pal, S. K.; Itkis, M. E.; Tham, F. S.; Reed, R. W.; Oakley, R. T.; Haddon, R. C. Trisphenalenyl-Based Neutral Radical Molecular Conductor. *J. Am. Chem. Soc.* **2008**, *130*, 3942.

[11] (a) Haddon, R. C.; Sarkar, A.; Pal, S. K.; Chi, X.; Itkis, M. E.; Tham, F. S. Localization of Spin and Charge in Phenalenyl-Based Neutral Radical Conductors. *J. Am. Chem. Soc*. **2008**, *130*, 13683. (b) Sarkar, A.; Pal, S. K.; Itkis, M. E.; Liao, P.; Tham, F. S.; Donnadieu, B.; Haddon, R. C. Methoxy-Substituted Phenalenyl-Based Neutral Radical Molecular Conductor. *Chem. Mater*. **2009**, *21*, 2226. (c) Bag, P.; Itkis, M. E.; Pal, S. K.; Donnadieu, B.; Tham, F. S.; Park, H.; Schlueter, J. A.; Siegrist, T.; Haddon, R. C. Resonating Valence Bond and σ-Charge Density Wave Phases

in a Benzannulated Phenalenyl Radical. *J. Am. Chem. Soc*. **2010**, *132*, 2684. (d) Bohlin, J.; Hansson, A.; Stafstrom, S. Electronic structure calculations of the phenalenyl-based neutral radical conductor bis(9-cyclohexylimino-1-phenalenyl) boron. *Phys. Rev. B* **2006**, *74*, 155111. (e) Bag, P.; Pal, S. K.; Itkis, M. E.; Sarkar, S.; Tham, F. S.; Donnadieu, B.; Haddon, R. C. Synthesis of Tetrachalcogenide-Substituted Phenalenyl Derivatives: Preparation and Solid-State Characterization of Bis(3,4,6,7-tetrathioalkyl-phenalenyl)boron Radicals. *J. Am. Chem. Soc.* **2013***, 135*, 12936.

[12] (a) Cordes, A. W.; Haddon, R. C.; Oakley, R. T. Heterocyclic thiazyl and selenazyl radicals; synthesis and applications in solid state architecture. In *The Chemistry of Inorganic Ring Systems*, Steudel, R., Ed.; Elsevier, Amsterdam; 1992, pp 295-321. (b) Oakley, R. T. Chemical binding within and between inorganic rings; the design and synthesis of molecular conductors. *Can. J. Chem*. **1993**, *71*, 1775.

[13] (a) Rawson, J. M.; Alberola, A.; Whalley, A. Thiazyl radicals: old materials for new molecular devices. *J. Mater. Chem.* **2006**, *16*, 2560. (b) Hicks, R. G. In *Stable Radicals: Fundamentals and Applied Aspects of Odd-Electron Compounds*; Hicks, R. G., Ed.; John Wiley & Sons, Ltd., Wiltshire, 2010 pp 317-380. (c) Ratera, I.; Veciana, J. Playing with organic radicals as building blocks for functional molecular materials. *Chem. Soc. Rev*. **2012**, *41*, 303. (d) Boeré, R. T.; Roemmele, T. L. Chalcogen-Nitrogen Radicals. *Comp. Inorg. Chem*. *II* **2013**, *1*, 375. (e) Rawson, J. M.; Hayward, J. J. In *Handbook of Chalcogen Chemistry: New Perspectives in Sulfur, Selenium and Tellurium*; Devillanova, F. and Du Mont, W.-W., Eds.; Royal Society of Chemistry: Cambridge, 2013; Vol 2; pp 69-98.

[14] (a) Bendikov, M.; Wudl, F.; Perepichka, D. F. *Chem. Rev.* **2004**, *104*, 4891. (b) Cortizo-Lacalle, D.; Skabara, P. J.; Westgate, T. D. *Handbook of Chalcogen Chemistry: New Perspectives in Sulfur, Selenium and Tellurium*; Devillanova, F. and Du Mont, W.-W., Eds.; Royal Society of Chemistry: Cambridge, 2013; Vol 2; pp 99-126.

[15] (a) Clarke, C. S.; Haynes, D. A; Smith, J. N. B.; Batsanov, A. S.; Howard, J. A. K.; Pascu, S. I.; Rawson, J. M. The effect of fluorinated aryl substituents on the crystal structures of 1,2,3,5-dithiadiazolyl radicals. *CrystEngComm* **2010**, *12*, 172. (b) Beldjoudi, Y.; Arauzo, A.; Palacio, F.; Pilkington, M.; Rawson, J. M. Studies on a "Disappearing Polymorph": Thermal and Magnetic Characterization of *α*-*p*-NCC_6F_4CNSSN. *J. Am. Chem. Soc.* **2016**, *138*, 16779. (c) Rawson, J. M.;

Banister, A. J.; Lavender, I. The Chemistry of Dithiadiazolylium and Dithiadiazolyl Rings. *Adv. Heterocycl. Chem*. **1995**, *62*, 137. (d) Beldjoudi, Y.; Sun, R; Arauzo, A; Campo, J; Less, R. J.; Rawson, J. M. Structural Variations in the Dithiadiazolyl Radicals p-ROC$_6$F$_4$CNSSN (R = Me, Et, Pr-n, Bu-n): A Case Study of Reversible and Irreversible Phase Transitions in *p*-EtOC$_6$F$_4$CNSSN. *Cryst. Growth Des.* **2018**, *18*, 179.

[16] (a) Andrews, M. P.; Cordes, A. W.; Douglass, D. C.; Fleming, R. M.; Glarum, S. H.; Haddon, R. C.; Marsh, P.; Oakley, R. T.; Palstra, T.T.M.; Schneemeyer, L. F.; Trucks, G. W.; Tycko, R. W.; Waszczak, J. V.; Warren, W. W.; Young, K. M.; Zimmerman, N. M. One-Dimensional Stacking of Bifunctional Dithia- and Diselenadiazolyl Radicals; Preparation, Structural and Electronic Properties of 1,3-[(E$_2$N$_2$C)C$_6$H$_4$(CN$_2$E$_2$)] (E = S, Se). *J. Am. Chem. Soc.* **1991**, *113*, 3559. (b) Cordes, A. W.; Haddon, R. C.; Hicks, R. G.; Oakley, R. T.; Palstra, T. T. M.; Schneemeyer, L. F.; Waszczak, J. V. Polymorphism of 1,3-Phenylene Bis(diselenadiazolyl); Solid State Structural and Electronic Properties of *β*-1,3-[(Se$_2$N$_2$C)C$_6$H$_4$(CN$_2$Se$_2$)]. *J. Am. Chem. Soc.* **1992**, *114*, 1729. (c) Yong, W.; Lekin, K.; Bauer, R. P. C.; Tse, J. S.; Desgreniers, S.; Secco, R. A.; Hirao, N.; Oakley, R. T. Pancakes under Pressure: A Case Study on Isostructural Dithia- and Diselenadiazolyl Radical Dimers. *Inorg. Chem*. **2019**, *58*, 3550.

[17] (a) Bryan, C. D.; Cordes, A. W.; Fleming, R. M.; George, N. A.; Glarum, S. H.; Haddon, R. C.; MacKinnon, C. D.; Oakley, R. T.; Palstra, T. T. M.; Perel, A. S. Charge Transfer Salts of Benzene-bridged 1,2,3,5-Dithiadiazolyl Diradicals; Preparation, Structures and Transport Properties of 1,3- and 1,4-[(S$_2$N$_2$C)C$_6$H$_4$(CN$_2$S$_2$)][X] (X = I, Br). *J. Am. Chem. Soc*. **1995**, *117*, 6880. (b) Bryan, C. D.; Cordes, A. W.; Goddard, J. D.; Haddon, R. C.; Hicks, R. G.; MacKinnon, C. D.; Mawhinney, R. C.; Oakley, R. T.; Palstra, T. T. M.; Perel, A. S. Preparation and Characterization of the Disjoint Diradical 4,4′-Bis(1,2,3,5-dithiadiazolyl) [S$_2$N$_2$C-CN$_2$S$_2$] and its Iodine Charge Transfer Salt [S$_2$N$_2$C-CN$_2$S$_2$][I]. *J. Am. Chem. Soc.* **1996**, *118*, 330.

[18] Cordes, A. W.; Haddon, R. C.; Oakley, R. T. A Molecule like Sodium. *Phosphorus, Sulfur Silicon Relat. Elem.* **2004**, *179*, 673.

[19] (a) Beer, L.; Brusso, J. L.; Cordes, A. W.; Haddon, R. C.; Itkis, M. E.; Kirschbaum, K.; MacGregor, D. S.; Oakley, R. T.; Pinkerton, A. A.; Reed, R. W. Resonance-Stabilized 1,2,3-Dithiazolo-1,2,3-dithiazolyls as Neutral π-Radical Conductors. *J. Am. Chem. Soc*. **2002**, *124*, 9498. (b) Beer, L.; Britten, J. F.; Brusso, J. L.; Cordes, A. W.; Haddon, R. C.; Itkis, M. E.;

MacGregor, D. S.; Oakley, R. T.; Reed, R. W.; Robertson, C. M. Prototypal Dithiazolodithiazolyl Radicals: Synthesis, Structures, and Transport Properties. *J. Am. Chem. Soc*. **2003**, *125*, 14394. (c) Leitch, A. A.; Reed, R. W.; Robertson, C. M.; Britten, J. F.; Yu, X.; Secco, R. A.; Oakley, R. T. An Alternating π-Stacked Bisdithiazolyl Radical Conductor. *J. Am. Chem. Soc.* **2007**, *129*, 7903.

[20] (a) Brusso, J. L.; Derakhshan, S.; Itkis, M. E.; Kleinke, H.; Haddon, R. C.; Oakley, R. T.; Reed, R. W.; Richardson, J. F.; Robertson, C. M.; Thompson, L. K. Isostructural Bisdithiazolyl and Bisthiaselenazolyl Radicals: Trends in Bandwidth and Conductivity. *Inorg. Chem*. **2006**, *45*, 10958. (b) Brusso, J. L.; Cvrkalj, K.; Leitch, A. A.; Oakley, R. T.; Reed, R. W.; Robertson, C. M. Resonance Stabilized Bisdiselenazolyls as Neutral Radical Conductors. *J. Am. Chem. Soc*. **2006**, *128*, 15080. (c) Leitch, A. A.; Yu, X.; Winter, S. M.; Secco, R. A.; Dube, P. A.; Oakley, R. T. Structure and Property Correlations in Heavy Atom Radical Conductors. *J. Am. Chem. Soc*. **2009**, *131*, 7112.

[21] Leitch, A. A.; Lekin, K.; Winter, S. M.; Downie, L. E.; Tsuruda, H.; Tse, J. S.; Mito, M.; Desgreniers, S.; Dube, P. A.; Zhang, S.; Liu, Q.; Jin, C.; Ohishi, Y.; Oakley, R. T. From Magnets to Metals: The Response of Tetragonal Bisdiselenazolyl Radicals to Pressure. *J. Am. Chem. Soc*. **2011,** *133*, 6051.

[22] Winter, S. M.; Oakley, R. T.; Kovalev, A. E.; Hill, S. Spin-orbit effects in heavy-atom organic radical ferromagnets. *Phys. Rev. B.* **2012**, *85*, 094430.

[23] (a) Robertson, C. M.; Leitch, A. A.; Cvrkalj, K.; Reed, R. W.; Myles, D. J. T.; Dube, P. A.; Oakley, R. T. Enhanced Conductivity and Magnetic Ordering in Isostructural Heavy Atom Radicals. *J. Am. Chem. Soc*. **2008**, *130*, 8414. (b) Robertson, C. M.; Leitch, A. A.; Cvrkalj, K.; Myles, D. J. T.; Reed, R. W.; Dube, P. A.; Oakley, R. T. Ferromagnetic Ordering in Bisthiaselenazolyl Radicals: Variations on a Tetragonal Theme. *J. Am. Chem. Soc*. **2008**, *130*, 14791. (c) Leitch, A. A.; Brusso, J. L.; Cvrkalj, K.; Reed, R. W.; Robertson, C. M.; Dube, P. A.; Oakley, R. T. Spin-canting in heavy atom heterocyclic radicals. *Chem. Commun*. **2007**, 3368. (d) Lekin, K.; Ogata, K.; Maclean, A.; Mailman, A.; Winter, S. M.; Assoud, A.; Mito, M.; Tse, J. S.; Desgreniers, S.; Hirao, N.; Dube, P. A.; Oakley, R. T. Pushing T_C to 27.5 K in a heavy atom radical ferromagnet. *Chem. Commun*. **2016**, *52*, 13877. (e) Irie, K.; Shibayama, K.; Mito, M.; Takagi, S.; Ishizuka, M.; Lekin, K.; Oakley, R. T. High-pressure DC magnetic measurements on a

bisdiselenazolyl radical ferromagnet using a vibrating-coil SQUID magnetometer. *Phys. Rev. B* **2019**, *99*, 014417.

[24] Winter, S. M.; Hill, S.; Oakley, R. T. Magnetic Ordering and Anisotropy in Heavy Atom Radicals. *J. Am. Chem. Soc*. **2015**, *137*, 3720.

[25] (a) Yu, X.; Mailman, A.; Dube, P. A.; Assoud, A.; Oakley, R. T. The first semiquinone-bridged bisdithiazolyl radical conductor: a canted antiferromagnet displaying a spin-flop transition. *Chem. Commun*. **2011**, *47*, 4655. (b) Yu, X.; Mailman, A.; Lekin, K.; Assoud, A.; Dube, P. A.; Oakley, R. T. A Bimodal Oxobenzene-bridged Bisdithiazolyl Radical Conductor. *Cryst. Growth Des.* **2012**, *12*, 2485. (c) Yu, X.; Mailman, A.; Lekin, K.; Assoud, A.; Robertson, C. M.; Noll, B. C.; Campana, C. F.; Howard, J. A. K.; Dube, P. A.; Oakley, R. T. Semiquinone-Bridged Bisdithiazolyl Radicals as Neutral Radical Conductors. *J. Am. Chem. Soc*. **2012**, *134*, 2264. (d) Mailman, A.; Winter, S. M.; Yu, X.; Robertson, C. M.; Yong, W.; Tse, J. S.; Secco, R. A.; Liu, Z.; Dube, P. A.; Howard, J. A. K.; Oakley, R. T. Crossing the Insulator-to-Metal Barrier with a Thiazyl Radical Conductor. *J. Am. Chem. Soc*. **2012**, *134*, 9886. (e) Wong, J. W. L.; Mailman, A.; Winter, S. M.; Robertson, C. M.; Holmberg, R. J.; Murugesu, M.; Dube, P. A.; Oakley, R. T. Supramolecular architecture, crystal structure and transport properties of the prototypal oxobenzene-bridged bisdithiazolyl radical conductor. *Chem. Commun*. **2014**, *50*, 785.

[26] (a) Winter, S. M.; Mailman, A.; Oakley, R. T.; Thirunavukkuarasu, K.; Hill, S.; Graf, D. E.; Tozer, S. W.; Tse, J. S.; Mito, M.; Yamaguchi, H. Electronic and Magnetic Structure of Neutral Radical FBBO. *Phys. Rev. B* **2014**, *89*, 214403. (b) Mailman, A.; Winter, S. M.; Wong, J. W. L.; Robertson, C. M.; Assoud, A.; Dube, P. A.; Oakley, R. T. Multiple Orbital Effects and Magnetic Ordering in a Neutral Radical. *J. Am. Chem. Soc*. **2015**, *137*, 1044.

[27] Mailman, A.; Wong, J. W. L.; Winter, S. M.; Claridge, R. C. M.; Robertson, C. M.; Assoud, A.; Yong, W.; Steven, E.; Dube, P. A.; Tse, J. S.; Desgreniers, S.; Secco, R. A.; Oakley, R. T. Fine Tuning the Performance of Multiorbital Radical Conductors by Substituent Effects. *J. Am. Chem. Soc*. **2017**, *139*, 1625.

[28] The study of multi-orbital effects has a long history, going back to the exploration of ferromagnetic exchange by virtual hopping between the SOMO and an empty orbital in inorganic oxides. See (a) Anderson, P. W. New Approach to the Theory of Superexchange Interactions. *Phys. Rev.* **1959**, *115*, 2. (b) Goodenough, J. B. An interpretation of the magnetic properties of the

perovskite-type mixed crystals $La_{1-x}Sr_xCoO_{3-\lambda}$. *J. Phys. Chem. Solids* **1958**, *6*, 287. (c) Goodenough, J. B. Magnetism and the Chemical Bond; Interscience-Wiley: New York, 1963.

[29] (a) Wong, J. W. L.; Mailman, A.; Lekin, K.; Winter, S. M.; Yong, W.; Zhao, J.; Garimella, S. V.; Tse, J. S.; Secco, R. A.; Desgreniers, S.; Ohishi, Y.; Borondics, F.; Oakley, R. T. Pressure Induced Phase Transitions and Metallization of a Neutral Radical Conductor. *J. Am. Chem. Soc*. **2014**, *136*, 1070. (b) Tian, D.; Winter, S. M.; Mailman, A.; Wong, J. W. L.; Yong, W.; Yamaguchi, H.; Jia, Y.; Tse, J. S.; Desgreniers, S.; Secco, R. A.; Julian, S. R.; Jin, C.; Mito, M.; Ohishi, Y.; Oakley, R. T. The Metallic State in Neutral Radical Conductors: Dimensionality, Pressure and Multiple Orbital Effects. *J. Am. Chem. Soc*. **2015**, *137*,14136.

[30] Boeré, R. T.; Moock, K. H. Solution Disproportionation Energies of 1,2,3,5-Dithia- and Diselenadiazoles. Direct Comparison of Solution Oxidation Potentials with Ionization Energies in the Gas Phase. J. *Am. Chem. Soc*. **1995**, *117*, 4755.

[31] (a) Alcock, N. W. Secondary Bonding to Nonmetallic Elements. *Adv. Inorg. Chem. Radiochem*. **1972**, *15*, 1. (b) Brammer, L. Halogen Bonding, Chalcogen Bonding, Pnictogen Bonding, Tetrel Bonding: Origins, Current Status and Discussion. *Faraday Discuss.* **2017**, *203*, 485. (c) Desiraju, G. R. Supramolecular Synthons in Crystal Engineering - a New Organic Synthesis. *Angew. Chem., Int. Ed. Engl.* **1995**, *34*, 2311. (d) Desiraju, G. R. Crystal Engineering: From Molecule to Crystal. *J. Am. Chem. Soc.* **2013**, *135*, 9952.

[32] (a) Haddon, R. C.; Chi, X.; Itkis, M. E.; Anthony, J. E.; Eaton, D. L.; Siegrist, T.; Mattheus, C. C.; Palstra, T. T. M. Band Electronic Structure of One- and Two-Dimensional Pentacene Molecular Crystals. *J. Phys. Chem. B* **2002**, *106*, 8288. (b) Payne, M. M.; Parkin, S. R.; Anthony, J. E.; Kuo, C.-C.; Jackson, T. N. Organic Field-Effect Transistors from Solution-Deposited Functionalized Acenes with Mobilities as High as 1 $cm^2/V{\cdot}s$. *J. Am. Chem. Soc.* **2005**, *127*, 4986. (c) Dong, H.; Wang, C.; Hu, W. High Performance Organic Semiconductors for Field-Effect Transistors. *Chem. Commun.* **2010**, *46*, 5211. (d) He, T.; Stolte, M.; Burschka, C.; Hansen, N. H.; Musiol, T.; Kälblein, D.; Pflaum, J.; Tao, X.; Brill, J.; Würthner, F. Single-Crystal Field-Effect Transistors of New Cl_2-NDI Polymorph Processed by Sublimation in Air. *Nat. Comm*. **2015**, *6*, 5954. (e) Wang, C.; Dong, H.; Li, H.; Zhao, H.; Meng, Q.; Hu, W. Dibenzothiophene Derivatives: From Herringbone to Lamellar Packing Motif. *Crys. Growth Des*. **2010**, *10*, 4155. (f) Kwon, T.;

Koo, J. Y.; Choi, H. C. Surface-Mediated Recrystallization for Highly Conducting Organic Radical Crystal. *Crys. Growth Des*. **2019**, *19*, 551.

[33] (a) Mailman, A.; Leitch, A. A.; Yong, W.; Steven, E.; Winter, S. M.; Claridge, R. C. M.; Assoud, A.; Tse, J. S.; Desgreniers, S.; Secco, R. A.; Oakley, R. T. The Power of Packing: Metallization of an Organic Semiconductor. *J. Am. Chem. Soc.* **2017**, *139*, 2180. (b) Lekin, K.; Leitch, A. A.; Assoud, A.; Yong, W.; Desmarais, J.; Tse, J. S.; Desgreniers, S.; Secco, R. A.; Oakley, R. T. Benzoquinone-Bridged Heterocyclic Zwitterions as Building Blocks for Molecular Semiconductors and Metals. *Inorg. Chem.* **2018**, *57*, 4757.

[34] (a) Warburton, W. K. Arylthiazathiolium Salts and *o*-Aminoaryl Thiols - The Herz Reaction. *Chem. Rev*. **1957**, *57*, 1011. (b) Rakitin, O. A.; Zibarev, A. V. Synthesis and Applications of 5-Membered Chalcogen-Nitrogen π-Heterocycles with Three Heteroatoms. *Asian. J. Chem*. **2018**, *7*, 2397.

[35] Winter, S. M.; Roberts, R. J.; Mailman, A.; Cvrkalj, K.; Assoud, A. Oakley, R. T. Thermal conversion of a pyridine-bridged bisdithiazolyl radical to a zwitterionic bisdithiazolopyridone. *Chem. Commun*. **2010**, *46*, 4496.

[36] (a) Bondi, A. Van der Waals Volumes and Radii. *J. Phys. Chem.* **1964**, *68*, 441. (b) Dance, I. Distance Criteria for Crystal Packing Analysis of Supramolecular Motifs. *New J. Chem*. **2003**, *27*, 22.

[37] (a) Hobza, P.; Selzle, H. L.; Schlag, E. W. Potential Energy Surface of the Benzene Dimer: Ab Initio Theoretical Study. *J. Am. Chem. Soc.* **1994**, *116*, 3500. (b) Gavezzotti, A.; Desiraju, G. R. A systematic analysis of packing energies and other packing parameters for fused-ring aromatic hydrocarbons. *Acta Crystallogr*. *B* **1988**, *44*, 427. (c) Bernstein, J.; Sarma, J. A. R. P.; Gavezzotti, A. Generation of unknown crystal phases for aromatic hydrocarbons by packing energy calculations. *Chem. Phys. Lett*. **1990**, *174*, 361.

[38] (a) Schiødt, N. C.; Bjørnholm, T.; Bechgaard, K.; Neumeier, J. J.; Allgeier, C.; Jacobsen, C. S.; Thorup, N. Structural, electrical, magnetic, and optical properties of bis-benzene-1,2-dithiolato-Au(IV) crystals. *Phys. Rev. B* **1996**, *53*, 1773. (b) Belo, D.; Alves, H.; Lopes, E. B.; Duarte, M. T.; Gama, V.; Henriques, R. T.; Almeida, M.; Pérez-Benítez, A.; Rovira, C.; Veciana, J. Gold Complexes with Dithiothiophene Ligands: A Metal Based on a Neutral Molecule. *Chem.- Eur. J.*

2001, *7*, 511. (c) Dautel, O. J.; Fourmigué, M.; Canadell, E.; Auban-Senzier, P. Fluorine Segregation Controls the Solid-State Organization and Electronic Properties of Ni and Au Dithiolene Complexes: Stabilization of a Conducting Single-Component Gold Dithiolene Complex. *Adv. Funct. Mater.* **2002**, *12*, 693. (d) Tenn, N.; Bellec, N.; Jeannin, O.; Piekara-Sady, L.; Auban-Senzier, P.; Íñiguez, J; Canadell, E.; Lorcy, D. A Single-Component Molecular Metal Based on a Thiazole Dithiolate Gold Complex. *J. Am. Chem. Soc*. **2009**, *131*, 16961.

[39] (a) Le Gal, Y.; Roisnel, T.; Auban-Senzier, P.; Bellec, N.; Íñiguez, J.; Canadell, E.; Lorcy, D. Stable Metallic State of a Neutral-Radical Single-Component Conductor at Ambient Pressure. *J. Am. Chem. Soc.* **2018**, *140*, 2998. (b) Brière, B.; Caillaux, J.; Le Gal, Y.; Lorcy, D.; Lupi, S.; Perucchi, A.; Zaghrioui, M.; Soret, J. C.; Sopracase, R.; Ta Phuoc, V. Interplay between bandwidth-controlled and filling-controlled pressure-induced Mott insulator to metal transition in the molecular compound [Au(Et-thiazdt)$_2$]. *Phys. Rev B.* **2018**, *97*, 035101.

[40] Zincke, Th.; Glahn, W. Über Versuche zur Darstellung chinoider Schwefelverbindungen *Ber. Dtsch. Chem. Ges.* **1907**, *40*, 3039.

[41] Boeré, R. T.; Moock, K. H.; Parvez, M. Electrochemical evidence for the existence of three stable oxidation states for heterocycle of the type $XC_6H_4CN_2E_2$ (E = S, Se). X-ray crystal structure of the dimer with X = Cl, E = S. *Z. Anorg. Allg. Chem.* **1994**, *620*, 1589.

[42] WinEPR Simfonia, version 1.25; Bruker Instruments, Inc., Billerica, MA, 1996.

[43] *CrystalClear*; Rigaku Corporation: Tokyo, Japan, 2005.

[44] *APEX2*; Bruker AXS Inc.: Madison, WI, 2007.

[45] *SADABS*; Bruker AXS Inc.: Madison, WI, 2001.

[46] Dolomanov, O. V.; Bourhis, L. J.; Gildea, R. J.; Howard, J. A. K.; Puschmann, H. OLEX2: a complete structure solution, refinement and analysis program. *J. Appl. Cryst*. **2009**, *42*, 339.

[47] (a) Carlin, R. L. In *Magnetochemistry*, Springer-Verlag, New York, 1986. (b) Bain, G. A.; Berry, J. F. Diamagnetic Corrections and Pascal's Constants. *J. Chem. Educ*. **2008**, *85*, 532.

[48] Giannozzi, P.; Baroni, S.; Bonini, N.; Calandra, M.; Car, R.; Cavazzoni, C.; Ceresoli, D.; Chiarotti, G. L.; Cococcioni, M.; Dabo, I.; Dal Corso, A.; Fabris, S.; Fratesi, G.; de Gironcoli, S.; Gebauer, R.; Gerstmann, U.; Gougoussis, C.; Kokalj, A.; Lazzeri, M.; Martin-Samos, L.; Marzari,

N.; Mauri, F.; Mazzarello, R.; Paolini, S.; Pasquarello, A.; Paulatto, L.; Sbraccia, C.; Scandolo, S.; Sclauzero, G.; Seitsonen, A. P.; Smogunov, A.; Umari, P.; Wentzcovitch, R. M. QUANTUM ESPRESSO: a modular and open-source software project for quantum simulations of materials. *J. Phys. Condens. Matter* **2009**, *21*, 395502.

[49] (a) Perdew, J.P.; Burke, K.; Ernzerhof, M. Generalized Gradient Approximation Made Simple. *Phys. Rev. Lett.* **1996**, *77*, 3865; *Phys. Rev. Lett*. **1997**, 78, 1396.

[50] Aroyo, M. I.; Orobengoa, D.; de la Flor, G.; Tasci, E. S.; Perez-Mato, J. M.; Wondratschek, H. Brillouin-Zone Database on the Bilbao Crystallographic Server. *Acta Crystallogr., Sect. A: Found. Adv.* **2014**, *70*, 126.

[51] (a) Mostofi, A. A.; Yates, J. R.; Lee, Y.-S.; Souza, I.; Vanderbilt, D.; Marzari, N. Wannier90: A tool for obtaining maximally-localised Wannier functions. *Comput. Phys. Commun*. **2008**, *178*, 685. (b) Souza, I.; Marzari, N.; Vanderbilt, N. Maximally localized Wannier functions for entangled energy bands. *Phys. Rev. B* **2001**, *65*, 035109.

Table of Contents Graphic

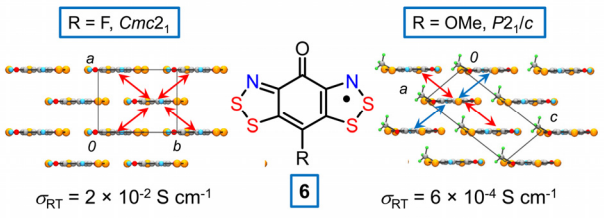

Despite seemingly similar brick-wall packing motifs, the reduction in electronic dimensionality between the multi-orbital radicals **6** with R = F (space group $Cmc2_1$) and R = OMe (space group $P2_1/c$) decreases the kinetic stabilization energy of the metallic state of the latter and lowers its conductivity.